Floquet topological phase transition in the α-$\mathcal{T}_3$ lattice

Bashab Dey and Tarun Kanti Ghosh
Department of Physics, Indian Institute of Technology-Kanpur, Kanpur-208 016, India

(Received 12 February 2019; published 22 May 2019)

We investigate topological characteristics of the photon-dressed band structure of the α-$\mathcal{T}_3$ lattice on being driven by off-resonant circularly polarized radiation. We obtain exact analytical expressions of the quasienergy bands over the first Brillouin zone. The broken time-reversal symmetry caused by the circularly polarized light lifts the triple point degeneracy completely at both the Dirac points. The gaps become unequal at **K** and **K**′ (except at $\alpha = 0$ and 1), which reveals the absence of inversion symmetry in the system. At $\alpha = 1/\sqrt{2}$, the gap between the flat and valence bands closes at **K**, while that between the conduction and flat bands closes at **K**′, thereby restoring a semimetalic phase. At the gap closing point ($\alpha = 1/\sqrt{2}$) which is independent of the radiation amplitude, there is a reappearance of low-energy Dirac cones around **K** and **K**′ points. Under the influence of the circularly polarized radiation, the α-$\mathcal{T}_3$ lattice is transformed from semimetal to a Haldane-like Chern insulator characterized by nonzero Chern number. The system undergoes a topological phase transition from $\mathcal{C} = 1(-1)$ to $\mathcal{C} = 2(-2)$ at $\alpha = 1/\sqrt{2}$, where $\mathcal{C}$ is the Chern number of the valence (conduction) band. This sets an example of a multiband system having larger Chern number. These results are supported by the appearance of chiral edge states in an irradiated α-$\mathcal{T}_3$ nanoribbon.

DOI: 10.1103/PhysRevB.99.205429

I. INTRODUCTION

Nontrivial topological phases in electronic and photonic systems have drawn enormous interest since the discovery of quantum Hall effect [1]. Topological insulators (TIs) [2–4] are distinctive states of matter characterized by an insulating bulk gap and gapless chiral or helical edge/surface modes that are topologically protected [5–12]. There are several classes of TIs, each of which is represented by a topological index. Chern insulators (CIs), also known as anomalous quantum Hall insulators (AQHIs) belong to a class of TIs characterized by a topological invariant called Chern number $\mathcal{C}$ associated with each band. A band with nonzero $\mathcal{C}$ gives rise to quantized Hall conductance even in the absence of a net magnetic flux. This feature was first predicted in an exotic 2D lattice model with broken time-reversal (TRS) symmetry, popularly known as the Haldane model [8] and was later verified experimentally [13]. These materials host chiral edge states (unidirectional propagating modes along an edge) that are robust against backscattering. The edge states are guaranteed by a nonzero Chern number of the bulk band through bulk-edge correspondence [14]. On the other hand, $\mathbb{Z}_2$ TIs, also called quantum spin Hall insulators (QSHIs), constitute another class of TIs in which the edge states are protected by time-reversal symmetry [5,6]. $\mathbb{Z}_2$ phases have been studied in large number of systems including two-dimensional (2D) quantum materials, strong spin-orbit coupled quantum wells and exotic lattice models. The gapless edge states in $\mathbb{Z}_2$ TIs are helical, i.e., they form pairs of counter-propagating modes with opposite spins along an edge, that are time-reversed copies of each other. The topology of these edge states is described by another topological invariant called the $\mathbb{Z}_2$ index. The topological phases exist in static [15] as well as in time-periodic systems [16–22]. Such a periodic drive can also transform a topologically trivial insulator to a CI [23,24]. The properties of periodically driven systems can be analyzed using Floquet theory [25,26].

The Chern number, in principle, can have any integral value. Most of the theoretically and experimentally studied CIs have Chern number $\mathcal{C} = 1$. Therefore it would be interesting to have a system with Chern number $\mathcal{C} \geqslant 2$. Recently, large Chern numbers have been predicted [27] and experimentally [28] realized in photonic 2D square and hexagonal crystals.

The α-$\mathcal{T}_3$ lattice, as shown in Fig. 1, is the extension of a honeycomb lattice. This is a conventional honeycomb lattice with two lattice points (A,B) and an additional lattice point (C) at the center of each honeycomb cell. The quasiparticle can hop from C sites to the alternate vertices (say, B) of the same honeycomb lattice. The hopping amplitude between A and B sites is $\tau \cos\phi$ and that between the B and C sites is $\tau \sin\phi$, where the angle ϕ parameterizes the hopping amplitude. It is convenient to express the angle ϕ by another parameter α such that $\alpha = \tan\phi$. For $\phi = 0$ ($\alpha = 0$), the C site is decoupled from the honeycomb lattice and it resembles to the monolayer graphene. The upper-left 2×2 matrix block in Eq. (1) describes the quasiparticle dynamics of monolayer graphene. For $\alpha = 1$ ($\phi = \pi/4$), the α-$\mathcal{T}_3$ model becomes conventional dice or $\mathcal{T}_3$ lattice having pseudospin-1 [29–36]. The α-$\mathcal{T}_3$ lattice with nonzero α has three energy bands since it has three sublattices consisting of a hub site (B) connected to six rim sites (A, C). The dice lattice can naturally be built by growing trilayers of cubic lattices (e.g.,$SrTiO_3/SrIrO_3/SrTiO_3$) in (111) direction [37]. It has been proposed theoretically that a dice lattice can be generated by interfering three counter-propagating pairs of identical laser beams [32] on a plane with wavelength $\lambda = 3a/2$, with a being the lattice constant. Later, it was shown that the α-$\mathcal{T}_3$ optical lattice can be achieved by dephasing one of the pairs

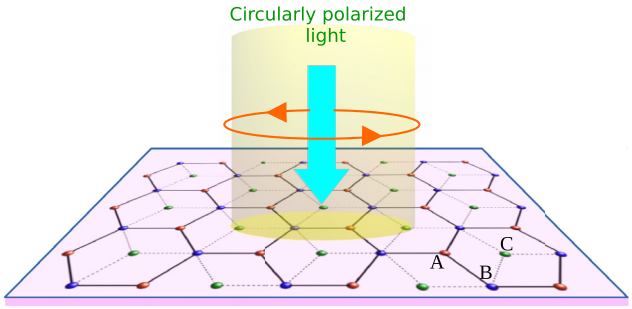

FIG. 1. Schematic diagram of the α-$\mathcal{T}_3$ lattice illuminated by off-resonant circularly polarized light.

of the laser beams while keeping other parameters unaltered [32,38]. Therefore a continuous change of α, through tuning phase of one of the three pairs of the laser beams, will allow us to study the changes in the topological properties of the system. The Hamiltonian of a $Hg_{1-x}Cd_xTe$ quantum well can be mapped to that of a low-energy α-$\mathcal{T}_3$ model with effective $\alpha = 1/\sqrt{3}$ on appropriate doping [39].

In recent years, there have been several studies [38,40–50] on various properties of the α-$\mathcal{T}_3$ lattice. The role of variable Berry phase in orbital susceptibility [38], magnetotransport coefficients [41] (quantized Hall conductivity and SdH oscillation) and optical conductivity [40] of the α-$\mathcal{T}_3$ lattice has been established. Very recently, Floquet states and the variable Berry phase dependent photoinduced gap in the α-$\mathcal{T}_3$ lattice irradiated by the circularly polarized on-resonant light have been studied in detail [45]. It has been shown that an off-resonant radiation induces a gap in graphene, on the surface states of TI [22], silicene [51], semi-Dirac systems [52], MoS_2 [53], etc. and transforms them to Chern insulating states. It is to be noted that the multiple Floquet bands formed by on-resonant light cannot be treated as a new static/effective band structure to determine the transport properties of such a nonequilibrium system, as shown by Kitagawa *et al.* [20]. A nonzero Chern number of any of these Floquet bands would not simply imply a quantized Hall conductance as there are additional contributions from photon-assisted electron conductions. However, on off-resonant (high-frequency) driving, the electrons cannot directly absorb or emit any photon; only its static band structure gets modified through virtual photon absorption-emission processes. So, the off-resonant condition provides an advantage to deal with systems strongly driven out of equilibrium and the transport properties of the system may be well approximated as those originating from the effective static band structure.

Since the proposal of Haldane's Chern insulator on a honeycomb lattice [8], several multiband CIs such as the kagome [10,54,55], dice [56], and Lieb [57] lattices with tunable parameters controlling the band topology have been studied. The α-$\mathcal{T}_3$ lattice is another example of a multiband system having trivial topology. In this work, we will show that an application of circularly polarized radiation on the α-$\mathcal{T}_3$ lattice makes it Haldane-type CI having nonzero Chern number and tuning the parameter α leads to a topological phase transitions at $\alpha = 1/\sqrt{2}$ by changing the Chern number of the valence (conduction) band from $\mathcal{C} = 1(-1)$ to larger Chern number $\mathcal{C} = 2(-2)$. This phase transition results in doubling of the number of chiral edge modes from one to two in the irradiated α-$\mathcal{T}_3$ nanoribbon. First we derive Floquet-Magnus Hamiltonian of the α-$\mathcal{T}_3$ lattice for the entire Brillouin zone. We get exact analytical expressions of quasienergy band structure over the full Brillouin zone. The triple-point degeneracy at the Dirac points is completely removed by breaking time-reversal symmetry due to time-periodic circularly polarized light. An intriguing state, independent of the radiation amplitude, appears at $\alpha = 1/\sqrt{2}$, where the gap between flat and valence bands closes at $\mathbf{K}$, while that between conduction and flat bands closes at $\mathbf{K}'$. The low-energy bands around both $\mathbf{K}$ and $\mathbf{K}'$ points display a Dirac-like dispersion with the reduced slope, as compared to monolayer graphene, at the gap closing points.

This paper is arranged as follows. In Sec. II, we provide topological band structure of the α-$\mathcal{T}_3$ lattice irradiated by the circularly polarized light. In Sec. III, we present the analytical calculations of the Chern number and show that the system undergoes a topological phase transition at $\alpha = 1/\sqrt{2}$. We present results of chiral edge states of an irradiated α-$\mathcal{T}_3$ nanoribbon in Sec. IV. In Sec. V, a summary and conclusion of our results are presented.

II. TOPOLOGICAL BAND STRUCTURE OF THE α-$\mathcal{T}_3$ LATTICE IRRADIATED BY CIRCULARLY POLARIZED LIGHT

Considering only the nearest-neighbor (NN) hopping integrals, the rescaled tight-binding Hamiltonian for the α-$\mathcal{T}_3$ lattice is given by

$$H_0(\mathbf{k}) = \begin{pmatrix} 0 & h(\mathbf{k})\cos\phi & 0 \\ h^*(\mathbf{k})\cos\phi & 0 & h(\mathbf{k})\sin\phi \\ 0 & h^*(\mathbf{k})\sin\phi & 0 \end{pmatrix}, \quad (1)$$

where $\mathbf{k} = (k_x, k_y)$ and $h(\mathbf{k}) = \tau(e^{i\mathbf{k}\cdot\boldsymbol{\delta}_1} + e^{i\mathbf{k}\cdot\boldsymbol{\delta}_2} + e^{i\mathbf{k}\cdot\boldsymbol{\delta}_3})$. Also, the three nearest neighbor position vectors with respect to the rim site B are $\boldsymbol{\delta}_1 = a(\sqrt{3}/2, -1/2)$, $\boldsymbol{\delta}_2 = a(-\sqrt{3}/2, -1/2)$ and $\boldsymbol{\delta}_3 = a(0, 1)$, with a is the lattice constant of graphene. The energy-wave-vector dispersion, independent of α, over the full Brillouin zone consists of three bands: two dispersive bands $E_\pm(\mathbf{k}) = \pm|h(\mathbf{k})|$ having electron-hole symmetry and a zero energy nondispersive band $E_0(\mathbf{k}) = 0$. The dispersion $E_\pm(\mathbf{k})$ is identical to that of graphene. The corresponding normalized eigenvectors over the full Brillouin zone are given by

$$\psi_{\mathbf{k},\pm} = \frac{1}{\sqrt{2}}\begin{pmatrix} \cos\phi e^{-i\psi(\mathbf{k})} \\ \pm 1 \\ \sin\phi e^{i\psi(\mathbf{k})} \end{pmatrix}, \quad \psi_{\mathbf{k},0} = \begin{pmatrix} \sin\phi e^{-i\psi(\mathbf{k})} \\ 0 \\ -\cos\phi e^{i\psi(\mathbf{k})} \end{pmatrix},$$

where $h(\mathbf{k}) = |h(\mathbf{k})|e^{-i\psi(\mathbf{k})}$. The low-energy quasiparticles in the α-$\mathcal{T}_3$ lattice are described by the two-dimensional (2D) Dirac-Weyl equation. It is a semimetalic system in absence of any external fields/perturbations. It will behave like a TI if a Haldane-type energy gap is induced at the Dirac points by external means. Next we show that circularly polarized off-resonant radiation opens up gaps and induces topological states in the α-$\mathcal{T}_3$ lattice.

The α-$\mathcal{T}_3$ lattice is irradiated with circularly polarized radiation falling normal to the lattice plane. The corresponding vector potential is $\mathbf{A}(t) = A_0(\cos\omega t, \sin\omega t)$, where $A_0 = E_0/\omega$ with E_0 and ω being the electric field amplitude and frequency of the radiation, respectively. By Pierl's substitution $\mathbf{k} \to (\mathbf{k} + e\mathbf{A}(t)/\hbar)$ in Eq. (1), we obtain

$$H(\mathbf{k},t) = \begin{pmatrix} 0 & h(\mathbf{k},t)\cos\phi & 0 \\ h^*(\mathbf{k},t)\cos\phi & 0 & h(\mathbf{k},t)\sin\phi \\ 0 & h^*(\mathbf{k},t)\sin\phi & 0 \end{pmatrix}, \tag{2}$$

where $h(\mathbf{k},t) = \tau\sum_{j=1}^{3} e^{i(\mathbf{k}+e\mathbf{A}(t)/\hbar)\cdot\boldsymbol{\delta}_j}$. The Hamiltonian $H(\mathbf{k},t)$ is periodic in time since $\mathbf{A}(t+T) = \mathbf{A}(t)$ with the periodicity $T = 2\pi/\omega$. Using the NN vectors $\boldsymbol{\delta}_j$ and the Jacobi-Anger expansion $e^{iz\sin\theta} = \sum_{n=-\infty}^{\infty} J_n(z)e^{in\theta}$ with $J_n(z)$ being the nth order cylindrical Bessel function, we get

$$h(\mathbf{k},t) = \tau\sum_{n=-\infty}^{\infty} J_n(\eta)[e^{in\omega t}e^{i\mathbf{k}\cdot\boldsymbol{\delta}_3} + e^{-in(\pi/3+\omega t)}e^{i\mathbf{k}\cdot\boldsymbol{\delta}_2} + e^{in(\pi/3-\omega t)}e^{i\mathbf{k}\cdot\boldsymbol{\delta}_1}].$$

Here, $\eta = eA_0a/\hbar$ is a dimensionless parameter characterizing the light intensity (can be expressed as square root of intensity and fine structure constant). Typically, $\eta \ll 1$ for the intensity of lasers and pulses available in the terahertz (THz) frequency domain. The off-resonant condition can be achieved when the photon energy is much larger than the band width of the undriven system, i.e., $\hbar\omega > 6\tau$. When the light frequency satisfies the off-resonant condition, the band structure is modified by the second-order virtual photon absorption-emission processes.

The effective time-independent Hamiltonian valid under off-resonant condition [58–60] is

$$H_{\text{eff}}(\mathbf{k}) = H_0(\mathbf{k}) + [H_-(\mathbf{k}), H_+(\mathbf{k})]/\hbar\omega + \mathcal{O}(1/\omega^2), \tag{3}$$

where

$$H_\pm(\mathbf{k}) = \frac{1}{T}\int_0^T dt\; e^{\mp i\omega t}H(\mathbf{k},t)$$

is the Fourier component of the Hamiltonian $H(\mathbf{k},t)$. By Fourier transform, we obtain

$$[H_-(\mathbf{k}), H_+(\mathbf{k})] = \frac{\Delta(\mathbf{k})}{2}S_z(\alpha), \tag{4}$$

where $S_z(\alpha)$ is defined as

$$S_z(\alpha) = 2\begin{pmatrix} \cos^2\phi & 0 & 0 \\ 0 & -\cos 2\phi & 0 \\ 0 & 0 & -\sin^2\phi \end{pmatrix} \tag{5}$$

and $\Delta(\mathbf{k}) = |g(\mathbf{k})|^2 - |f(\mathbf{k})|^2 = \hbar\omega\,\gamma(\mathbf{k})$ with

$$g(\mathbf{k}) = \tau J_1(\eta)[e^{i\mathbf{k}\cdot\boldsymbol{\delta}_1}e^{i\pi/3} + e^{i\mathbf{k}\cdot\boldsymbol{\delta}_2}e^{-i\pi/3} - e^{i\mathbf{k}\cdot\boldsymbol{\delta}_3}], \tag{6}$$

$$f(\mathbf{k}) = \tau J_1(\eta)[-e^{i\mathbf{k}\cdot\boldsymbol{\delta}_1}e^{-i\pi/3} - e^{i\mathbf{k}\cdot\boldsymbol{\delta}_2}e^{i\pi/3} + e^{i\mathbf{k}\cdot\boldsymbol{\delta}_3}]. \tag{7}$$

Hence, the light-matter coupling results in a mass term of the form $\gamma(\mathbf{k})S_z(\alpha)/2$ which lifts the threefold degeneracy at the Dirac points. It can be shown that the mass term reduces to $\mu\beta^2\hbar\omega S_z(\alpha)/2$ in the linearized low-energy limit where $\beta = 3\eta\tau/(2\hbar\omega)$ and $\mu = 1(-1)$ corresponds to $\mathbf{K}(\mathbf{K}')$ valleys. On time-reversal operation, $\gamma(\mathbf{k})$ changes sign, which implies the breaking of TRS in the system. Similarly, the term also changes sign on switching from right to left circular polarization. So, the mass term is trivially zero in case of linearly polarized light since it is a linear combination of both the polarizations with equal weights.

Interestingly, the mass term is Haldane-type which has opposite signs in the two valleys. It has been shown that the effective Hamiltonian in irradiated graphene under off-resonant condition can be mapped to the Haldane model with no sublatice potential and complex next-nearest-neighbor hoppings, which break TRS [20]. In Haldane model, the NN hoppings do not accumulate Aharonov-Bohm (AB) phases since the net magnetic flux through a unit cell is zero. In this model, the magnetic flux is locally zero everywhere on the lattice plane at a given time. However, the time-varying vector potential is spatially constant over the lattice, due to which NN hoppings acquire time-dependent AB phases.

The effective Hamiltonian (3) can now be written explicitly as

$$H_{\text{eff}}(\mathbf{k}) = \begin{pmatrix} \gamma(\mathbf{k})\cos^2\phi & h(\mathbf{k})\cos\phi & 0 \\ h^*(\mathbf{k})\cos\phi & -\gamma(\mathbf{k})\cos 2\phi & h(\mathbf{k})\sin\phi \\ 0 & h^*(\mathbf{k})\sin\phi & -\gamma(\mathbf{k})\sin^2\phi \end{pmatrix}. \tag{8}$$

The Hamiltonian $H_{\text{eff}}(\mathbf{k})$ satisfies the following anticommutation relations for $\alpha = 0$ and $\alpha = 1$:

$$\{H^G_{\text{eff}}(\mathbf{k}), \mathcal{P}_G\} = 0, \quad \{H^D_{\text{eff}}(\mathbf{k}), \mathcal{P}_D\} = 0. \tag{9}$$

Here, $\mathcal{P}_G$ and $\mathcal{P}_D$ are operators defined for graphene and dice, respectively, as follows:

$$\mathcal{P}_G = \mathcal{K}\begin{pmatrix} 0 & -1 & 0 \\ 1 & 0 & 0 \\ 0 & 0 & 1 \end{pmatrix}, \quad \mathcal{P}_D = \mathcal{K}\begin{pmatrix} 0 & 0 & -1 \\ 0 & 1 & 0 \\ -1 & 0 & 0 \end{pmatrix} \tag{10}$$

with $\mathcal{K}$ being the complex-conjugation operator. The relations (9) imply that a band with energy $\epsilon(\mathbf{k})$ will have a partner band with energy $-\epsilon(\mathbf{k})$. This symmetry confirms the presence of a zero-energy band in the three-band system. Hence, the flat band in dice lattice will not be perturbed by radiation. Also, the Hamiltonian is traceless, implying the sum of energies of the bands will be zero for all values of α.

The eigenvalues $\epsilon_m(\mathbf{k})$ of $H_{\text{eff}}(\mathbf{k})$ represent the off-resonant quasienergy band structure. The characteristic equation for the eigenvalue problem turns out to be a *depressed* cubic equation: $\lambda^3 + p\lambda + q = 0$, where

$$p = -\left[|h(\mathbf{k})|^2 + \gamma(\mathbf{k})^2\left(\cos^2 2\phi + \frac{\sin^2 2\phi}{4}\right)\right], \tag{11}$$

$$q = -\frac{\gamma(\mathbf{k})^3}{4}\sin^2 2\phi\cos 2\phi. \tag{12}$$

The eigenvalues are of the form

$$\epsilon_m(\mathbf{k}) = 2\sqrt{\frac{-p}{3}}\cos\left[\frac{1}{3}\cos^{-1}\left(\frac{3q}{2p}\sqrt{\frac{-3}{p}}\right) - \frac{2\pi m}{3}\right] \tag{13}$$

with $m = 0,\ 1$, and 2 correspond to the quasienergies of the conduction, flat and valence bands, respectively. The band

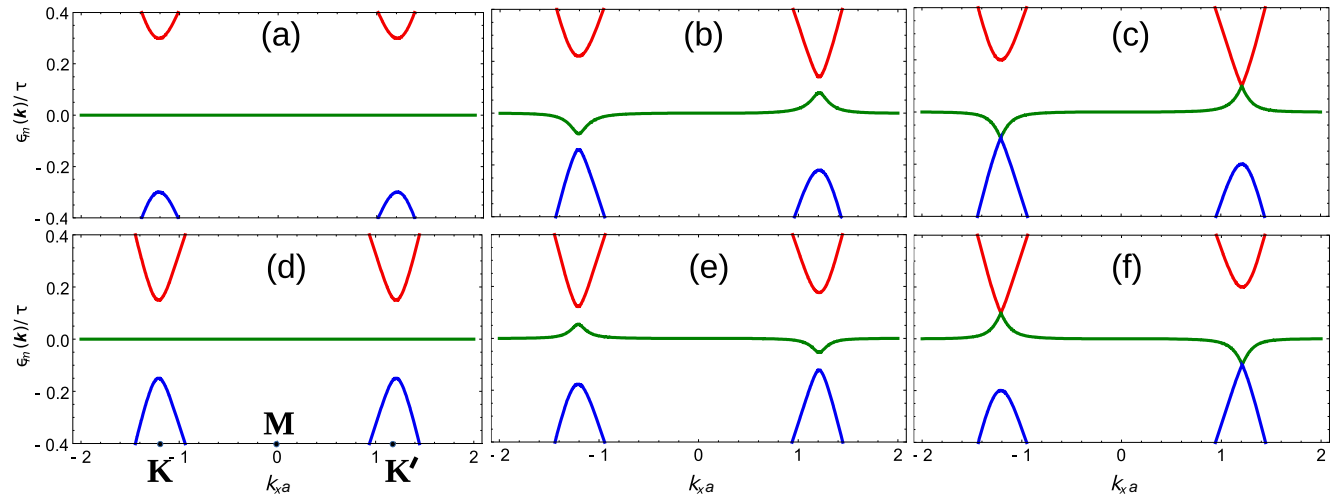

FIG. 2. Plots of low-energy Floquet bands for various values of α: (a) $\alpha = 0$, (b) 0.6, (c) $1/\sqrt{2}$, (d) 1, (e) 1.2, and (f) $\sqrt{2}$. The bands are plotted along the line joining the high-symmetry **K**, **M**, and **K**′ points. Bands are no longer symmetric under exchange of valleys except at $\alpha = 0$ and 1. Here we have taken $J_1(\eta) = 0.57$.

structure of the undriven α-$\mathcal{T}_3$ lattice is strongly modified by the off-resonant radiation and becomes α as well as η dependent. It exhibits interesting features as we tune α, which will be discussed in detail. The components of the normalized eigenvectors $|\Psi_m(\mathbf{k})\rangle = (a_m(\mathbf{k})\ \ b_m(\mathbf{k})\ \ c_m(\mathbf{k}))^T$ can be written as

$$a_m(\mathbf{k}) = \frac{d(\mathbf{k})\sin\theta\cos\phi e^{-i\psi(\mathbf{k})}}{\epsilon_m(\mathbf{k}) - d(\mathbf{k})\cos\theta\cos^2\phi} b_m(\mathbf{k}), \tag{14}$$

$$c_m(\mathbf{k}) = \frac{d(\mathbf{k})\sin\theta\sin\phi e^{i\psi(\mathbf{k})}}{\epsilon_m(\mathbf{k}) + d(\mathbf{k})\cos\theta\sin^2\phi} b_m(\mathbf{k}) \tag{15}$$

with

$$b_m(\mathbf{k}) = \Bigg[1 + \left(\frac{d(\mathbf{k})\sin\theta\cos\phi}{\epsilon_m(\mathbf{k}) - d(\mathbf{k})\cos\theta\cos^2\phi}\right)^2 + \left(\frac{d(\mathbf{k})\sin\theta\sin\phi}{\epsilon_m(\mathbf{k}) + d(\mathbf{k})\cos\theta\sin^2\phi}\right)^2\Bigg]^{-1/2}, \tag{16}$$

where we have parameterized $\gamma(\mathbf{k})$ and $h(\mathbf{k})$ as $\gamma(\mathbf{k}) = d(\mathbf{k})\cos\theta$, $h(\mathbf{k}) = d(\mathbf{k})\sin\theta e^{-i\psi(\mathbf{k})}$, with $d(\mathbf{k}) = \sqrt{|h(\mathbf{k})|^2 + \gamma(\mathbf{k})^2}$.

Now we shall analyze the topological band structures as we vary α continuously. Figure 2 shows the low-energy topological bands for different values of α in the first Brillouin zone. For three-band systems, there can be two distinct band gaps at the Dirac points: the gaps between the (i) conduction and flat bands ($\Delta_{\rm cf}^{\mathbf{K}/\mathbf{K}'}$) and (ii) flat and valence bands ($\Delta_{\rm fv}^{\mathbf{K}/\mathbf{K}'}$) at $\mathbf{K}/\mathbf{K}'$ points. In presence of TRS breaking circularly polarized light, the triple point degeneracy at both the Dirac points is completely lifted (i.e., $\Delta_{\rm cf}^{\mathbf{K}/\mathbf{K}'} \neq 0$ and $\Delta_{\rm fv}^{\mathbf{K}/\mathbf{K}'} \neq 0$) except at $\alpha = 1/\sqrt{2}$. The photoinduced gaps at $\alpha = 0$ and 1 are $\Delta_{\rm cf}^{\mathbf{K}/\mathbf{K}'} = \Delta_{\rm fv}^{\mathbf{K}/\mathbf{K}'} = \beta^2\hbar\omega$ and $\Delta_{\rm cf}^{\mathbf{K}/\mathbf{K}'} = \Delta_{\rm fv}^{\mathbf{K}/\mathbf{K}'} = \beta^2\hbar\omega/2$, respectively. It is interesting to note that $\Delta_{\rm cf}^{\mathbf{K}} = 0$ but $\Delta_{\rm fv}^{\mathbf{K}} \neq 0$ and $\Delta_{\rm cf}^{\mathbf{K}'} \neq 0$ but $\Delta_{\rm fv}^{\mathbf{K}'} = 0$ at $\alpha = 1/\sqrt{2}$. It implies that the band gaps at the Dirac points do not open completely at $\alpha = 1/\sqrt{2}$. Note that this result is independent of the radiation amplitude η (as long as the off-resonant approximation is valid). The partial closing of the band gap at $\alpha = 1/\sqrt{2}$ can be deduced by obtaining the eigenvalues at a Dirac point (say **K**) viz. $\epsilon_0 = \cos^2\phi$, $\epsilon_1 = -\cos 2\phi$, $\epsilon_2 = -\sin^2\phi$. Equating ϵ_0 with ϵ_1, we find that the band touching occurs at $\alpha = 1/\sqrt{2}$. We present plots of $\Delta_{\rm cf}^{\mathbf{K}}$ and $\Delta_{\rm fv}^{\mathbf{K}}$ versus α in Fig. 3. The system exhibits an interesting property of $\alpha \to 1/\alpha$ duality. The measurable quantities of the system will be same for α and $1/\alpha$. Hence, similar gap closing is also seen at $\alpha = \sqrt{2}$. However, the duality exchanges the Dirac points i.e., $\Delta_{\rm cf}^{\mathbf{K}}(\alpha) = \Delta_{\rm cf}^{\mathbf{K}'}(1/\alpha)$ and $\Delta_{\rm fv}^{\mathbf{K}}(\alpha) = \Delta_{\rm fv}^{\mathbf{K}'}(1/\alpha)$. The band gaps (in units of $\beta^2\hbar\omega$) at the Dirac point **K** are tabulated in Table I. For **K**′ point, one can easily check that $\Delta_{\rm cf}^{\mathbf{K}'} = \Delta_{\rm fv}^{\mathbf{K}}$ and $\Delta_{\rm fv}^{\mathbf{K}'} = \Delta_{\rm cf}^{\mathbf{K}}$ for given α.

Substituting $\mathbf{k} = \mathbf{K} + \mathbf{q}$ with $\mathbf{q} \to 0$ in Eq. (8), we get the low-energy Hamiltonian around **K**. Interestingly, the touching bands, i.e., flat and conduction bands, exhibit Dirac cones in the low-energy limit as

$$\epsilon_{0,1}(\mathbf{q}) = \frac{\beta^2\hbar\omega}{3} \pm \frac{\hbar v_f}{\sqrt{3}}|\mathbf{q}|.$$

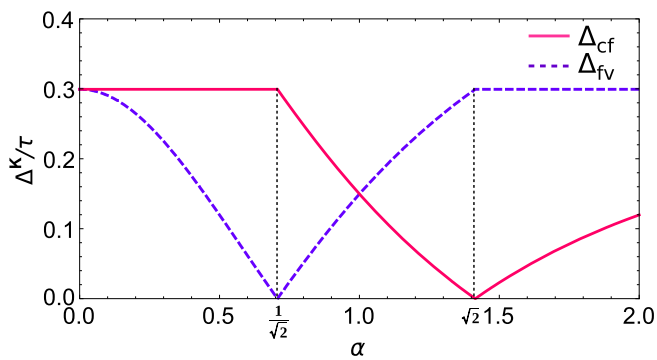

FIG. 3. Plots of the photoinduced gaps at the Dirac point **K** as a function of α.

TABLE I. Photoinduced gaps at the Dirac point **K** as a function of α.

Gaps	$0 \leqslant \alpha \leqslant 1/\sqrt{2}$	$1/\sqrt{2} \leqslant \alpha \leqslant \sqrt{2}$	$\alpha \geqslant \sqrt{2}$
$\Delta_{\rm cf}^{\mathbf{K}}$	1	$\cos^2\phi + \cos 2\phi$	$-(\cos 2\phi + \cos^2\phi)$
$\Delta_{\rm fv}^{\mathbf{K}}$	$-\sin^2\phi + \cos 2\phi$	$\sin^2\phi - \cos 2\phi$	1

It is to be noted that in the field free case, $\epsilon_m(\mathbf{k}) = \epsilon_m(-\mathbf{k})$ for all values of α. However, for the irradiated model, we have $\epsilon_m(\mathbf{k}) = \epsilon_m(-\mathbf{k})$ for $\alpha = 0,\ 1$ and $\epsilon_m(-\mathbf{k}) \neq \epsilon_m(\mathbf{k})$ for $\alpha \neq 0,\ 1$. This can be explained as follows − In the radiation-free case, the Kramer's degeneracy ensured by TRS guarantees $\epsilon_m(\mathbf{k}) = \epsilon_m(-\mathbf{k})$ irrespective of the value of α or other symmetries. On application of TRS-breaking circularly polarized light, the Kramer's degeneracy is lifted. Now, the band structure will be an even function in $\mathbf{k}$ only if the lattice has inversion symmetry (IS). Since graphene and dice lattice have IS, the band structure remains an even function in quasimomentum despite a broken TRS.

The topology of the band structure remains same if the energy gap in the band structure does not close and reopen while tuning the parameter continuously. Here we have seen that one of the gaps closes at $\alpha = 1/\sqrt{2}$ and reopens when $1/\sqrt{2} < \alpha < \sqrt{2}$. Hence, we expect a transition in band topology at $\alpha = 1/\sqrt{2}$. In 2D, a change in the Chern number or TKNN integer can be used to identify whether the system undergoes a topological transition or not. In the next section, we show that there is indeed a topological phase transition at $\alpha = 1/\sqrt{2}$ (equivalently at $\alpha = \sqrt{2}$) by evaluating the Chern number explicitly as a function of α.

III. CALCULATIONS OF THE CHERN NUMBER AND TOPOLOGICAL PHASE TRANSITIONS

We need to analyze the behavior of the Berry connection and Berry curvature in order to calculate the Chern number of each band analytically [61–63] as well as numerically [64]. The Berry connection for the band $\epsilon_m(\mathbf{k})$ can be written as $\mathbf{A}_m(\mathbf{k}) = i\langle\Psi_m(\mathbf{k})|\nabla_{\mathbf{k}}|\Psi_m(\mathbf{k})\rangle$. Under the gauge used in (14) and (15), the Berry connection reduces to

$$\mathbf{A}_m(\mathbf{k}) = s_m(\mathbf{k})\nabla_{\mathbf{k}}\psi(\mathbf{k}), \tag{17}$$

with $s_m(\mathbf{k}) = [|a_m(\mathbf{k})|^2 - |c_m(\mathbf{k})|^2]$. The Berry curvature of the mth band is defined as

$$\Omega_m(\mathbf{k}) = \hat{\mathbf{z}} \cdot [\nabla_{\mathbf{k}} \times \mathbf{A}_m(\mathbf{k})]. \tag{18}$$

Figure 4 shows the plots of $\Omega_2(\mathbf{k})$ around the two valleys for three values of α. The distribution of $\Omega_2(\mathbf{k})$ in graphene [Figs. 4(a) and 4(b)] is identical in the two valleys. Since $\mathbf{K} = -\mathbf{K}'$, $\Omega_2(\mathbf{k})$ is an even function indicating the presence of inversion (IS) symmetry in the lattice, but a broken TRS. This also holds true for $\alpha = 1$, i.e., dice lattice [Figs. 4(e) and 4(f)]. However, for $\alpha = 0.5$, $\Omega_2(\mathbf{k})$ is largely different in the two valleys [Figs. 4(d) and 4(e)]. This is a signature of the absence of IS and a broken TRS.

The Berry connection depends on the gauge and may have singularities within the first Brillouin zone (FBZ). The Berry curvature of the mth band is well defined when the quasienergy $\epsilon_m(\mathbf{k})$ is nondegenerate (i.e., mth band does not touch any other bands) for all values of $\mathbf{k}$ within the FBZ. Contour plots of the Berry curvature near the two Dirac points $\mathbf{K}$ and $\mathbf{K}'$ for different values of α are shown in Fig. 4. The surface integral of the Berry curvature $\Omega_m(\mathbf{k})$ over the FBZ gives $2\pi\mathcal{C}_m$, where $\mathcal{C}_m$ is an integer called the Chern number or TKNN index [65] for the mth band:

$$\mathcal{C}_m = \frac{1}{2\pi}\int_{\rm FBZ} \hat{\mathbf{z}} \cdot [\nabla_{\mathbf{k}} \times \mathbf{A}_m(\mathbf{k})]\, d^2\mathbf{k}. \tag{19}$$

It is important to mention here that any contributions due to gauge-dependent singularities in $\mathbf{A}_m(\mathbf{k})$ must be excluded from the above equation. If a global gauge transformation removes all the singularities, then Chern number of the band will be trivially zero by Stokes theorem. Note that $\mathcal{C}_m \neq 0$ implies the absence of a global gauge under which the Berry connection has no singularities in the FBZ. The Berry connection $\mathbf{A}_m(\mathbf{k})$ given in Eq. (17) is proportional to $\nabla_{\mathbf{k}}\psi(\mathbf{k})$. The gauge-dependent singularities in the Berry connection $\mathbf{A}_m(\mathbf{k})$ arise at the $\mathbf{k}$ points where the phase $\psi(\mathbf{k})$ of the off-diagonal matrix elements $h(\mathbf{k})$ is ill defined. It occurs if the function $h(\mathbf{k}) = 0$ for certain values of $\mathbf{k}$. In this band structure, since $h(\mathbf{K}) = h(\mathbf{K}') = 0$, $\psi(\mathbf{K})$ and $\psi(\mathbf{K}')$ are not defined and hence there may be singularity in $\mathbf{A}_m(\mathbf{k})$ at the Dirac points if $s_m(\mathbf{K}) \neq 0$ or $s_m(\mathbf{K}') \neq 0$. Thus we expect a nonzero Chern number in this case. First we calculate the Chern number for the valence band corresponding to $m = 2$. The variation $s_2(\mathbf{K})$ and $s_2(\mathbf{K}')$ with α is displayed in Fig. 5. Note that $s_2(\mathbf{K})$ and $s_2(\mathbf{K}')$ are evaluated very close to the Dirac points since they are not defined exactly at the Dirac points. These two functions can be written mathematically as

$$s_2(\mathbf{K}) = -\Theta(\alpha - 1/\sqrt{2}), \quad s_2(\mathbf{K}') = \Theta(\sqrt{2} - \alpha), \tag{20}$$

where $\Theta(x)$ is the usual unit step function.

Now we calculate the Chern number of the valence band for $\alpha < 1/\sqrt{2}$. Since $s_2(\mathbf{K}') = 1$ and $s_2(\mathbf{K}) = 0$, we have $\mathbf{A}_2(\mathbf{K}')$ not defined and $\mathbf{A}_2(\mathbf{K}) = 0$. For convenience, we remove the subscript **2** from $\mathbf{A}_2$, as we will stick to the quantities related to the valence band only. The Berry connection for valence band under the chosen gauge [say $\mathbf{A}_{\rm I}(\mathbf{k})$] has a singularity at $\mathbf{K}'$ point. Hence, $\mathbf{A}_{\rm I}(\mathbf{k})$ is not smoothly defined across the FBZ. We make a gauge transformation $\mathbf{A}_{\rm II}(\mathbf{k}) \to \mathbf{A}_{\rm I}(\mathbf{k}) - \nabla_{\mathbf{k}}\psi(\mathbf{k}) = [s_{\rm I}(\mathbf{k}) - 1]\nabla_{\mathbf{k}}\psi(\mathbf{k})$, which gives $\mathbf{A}_{\rm II}(\mathbf{K}') = 0$ and $\mathbf{A}_{\rm II}(\mathbf{K})$ not defined. In this gauge, $\mathbf{K}$ is the singular point. As long as there is a singularity under a given gauge, integral of the Berry curvature will not be defined if the gauge is chosen globally across the FBZ. So, we divide the FBZ, as depicted in Fig. 6, into two regions $R_{\rm I}$ and $R_{\rm II}$ surrounding $\mathbf{K}$ and $\mathbf{K}'$, respectively. We assign gauge-related Berry connections $\mathbf{A}_{\rm I}(\mathbf{k})$ and $\mathbf{A}_{\rm II}(\mathbf{k})$ in $R_{\rm I}$ and $R_{\rm II}$, respectively, so that the Berry curvature $[\Omega(\mathbf{k})]$ obtained from them is well-defined in each region. $\Gamma_{\rm I}$ and $\Gamma_{\rm II}$ are contours enclosing $R_{\rm I}$ and $R_{\rm II}$ respectively. The two regions share a common boundary coinciding with $\Gamma_{\rm I}$. Now, the Chern number can be written as

$$\begin{aligned}\mathcal{C}_2 &= \frac{1}{2\pi}\left[\int_{R_{\rm I}} \nabla_{\mathbf{k}} \times \mathbf{A}_{\rm I}(\mathbf{k}) + \int_{R_{\rm II}} \nabla_{\mathbf{k}} \times \mathbf{A}_{\rm II}(\mathbf{k})\right] \cdot \hat{\mathbf{z}} d^2\mathbf{k} \\ &= \frac{1}{2\pi}\left[\oint_{\Gamma_{\rm I}} \nabla_{\mathbf{k}}\psi(\mathbf{k}) \cdot d\mathbf{k}\right]\end{aligned} \tag{21}$$

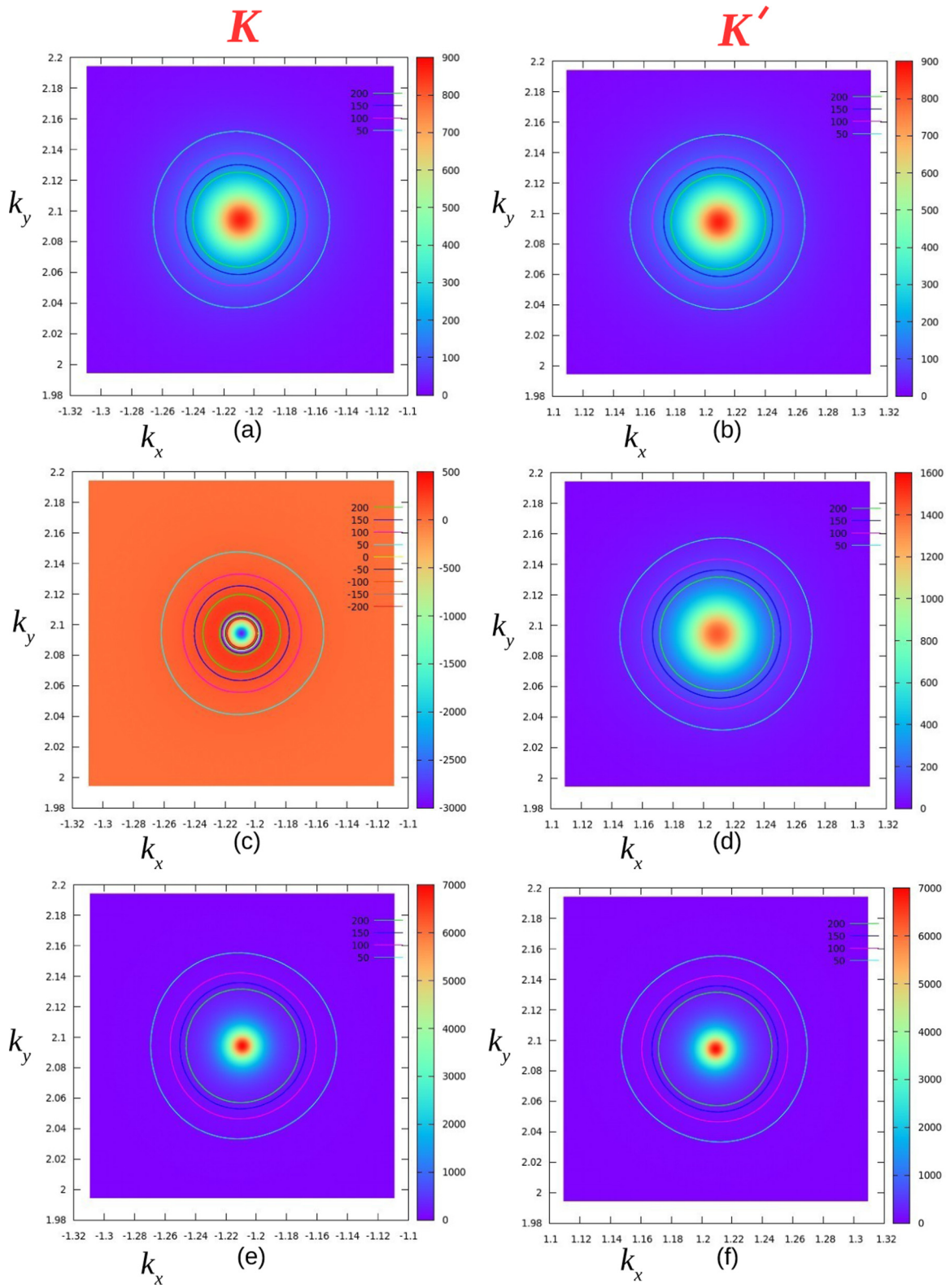

FIG. 4. Density-contour plots of the Berry curvature ($\Omega(\mathbf{k})$) around the two Dirac points $\mathbf{K}$ and $\mathbf{K}'$ for different values of α: (top) 0, (middle) 0.5, and (bottom) 1. Here, k_x and k_y are in units of a^{-1}.

where we have used the fact that integral along the outer boundary of $\Gamma_{\rm II}$ vanishes due to periodicity in $\mathbf{A}(\mathbf{k})$ across the FBZ. The region $R_{\rm I}$ can be chosen as an infinitesimally small circle around the Dirac point $\mathbf{K}$. Then, the term within the brackets is the vorticity $v_{\mathbf{K}}$ around $\mathbf{K}$ point. Since $v_{\mathbf{K}} = 2\pi$, $\mathcal{C}_2 = 1$. The valence band is degenerate with flat band at $\alpha = 1/\sqrt{2}$. Hence, the Chern number of the valence band at $\alpha = 1/\sqrt{2}$ is not defined.

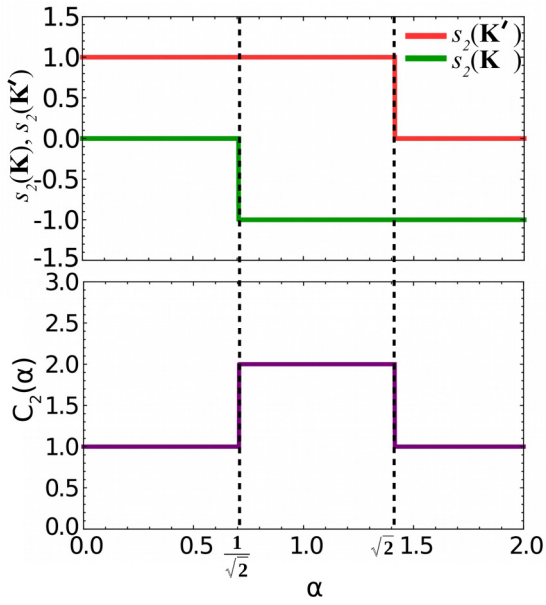

FIG. 5. (Top) Plots of $s_2(\mathbf{K})$ and $s_2(\mathbf{K}')$ vs α. (Bottom) Plots of the Chern number $\mathcal{C}_2$ vs α.

We have already seen that the three bands are nondegenerate again when α lying between $1/\sqrt{2}$ and $\sqrt{2}$, i.e., $1/\sqrt{2} < \alpha < \sqrt{2}$. In this case, $s_{\rm I}(\mathbf{K}') = 1$ and $s_{\rm I}(\mathbf{K}) = -1$. Hence, both $\mathbf{A}_{\rm I}(\mathbf{K})$ and $\mathbf{A}_{\rm I}(\mathbf{K}')$ are not defined. Since, we need at least one nonsingular point, this gauge choice is redundant. However, the gauge transformed $\mathbf{A}_{\rm II}(\mathbf{K}') = [s_{\rm I}(\mathbf{K}') - 1]\nabla_{\mathbf{k}}\psi(\mathbf{K}') = s_{\rm II}(\mathbf{K}')\nabla_{\mathbf{k}}\psi(\mathbf{K}') = 0$ and $\mathbf{A}_{\rm II}(\mathbf{K}) = [s_{\rm I}(\mathbf{K}) - 1]\nabla_{\mathbf{k}}\psi(\mathbf{K}) = s_{\rm II}(\mathbf{K})\nabla_{\mathbf{k}}\psi(\mathbf{K}) = -2\nabla_{\mathbf{k}}\psi(\mathbf{K})$. Thus, we have $s_{\rm II}(\mathbf{K}') = 0$ and $s_{\rm II}(\mathbf{K}) = -2$, i.e., $\mathbf{A}(\mathbf{k})$ is singular at $\mathbf{K}$ and is nonsingular at $\mathbf{K}'$. On making a gauge transformation $\mathbf{A}_{\rm III}(\mathbf{k}) \to \mathbf{A}_{\rm II}(\mathbf{k}) + 2\nabla_{\mathbf{k}}(\psi(\mathbf{k})) = [s_{\rm II}(\mathbf{k}) + 2)\nabla_{\mathbf{k}}\psi(\mathbf{k}) = s_{\rm III}(\mathbf{k})\nabla_{\mathbf{k}}\psi(\mathbf{k})$. Now, we have $s_{\rm III}(\mathbf{K}') = 2$ and $s_{\rm III}(\mathbf{K}) = 0$, i.e., $\mathbf{K}$ is nonsingular.

Again, we divide the BZ, similar to Fig. 6, into two regions $R_{\rm II}$ and $R_{\rm III}$ surrounding $\mathbf{K}'$ and $\mathbf{K}$, respectively. We assign gauge-related Berry connections $\mathbf{A}_{\rm II}(\mathbf{k})$ and $\mathbf{A}_{\rm III}(\mathbf{k})$ in $R_{\rm II}$ and $R_{\rm III}$, respectively, such that that $\Omega(\mathbf{k})$ is well-defined in each region. So, the Chern number is given by

$$\mathcal{C}_2 = \frac{1}{2\pi}\left[\int_{R_{\rm II}} \nabla_{\mathbf{k}} \times \mathbf{A}_{\rm II}(\mathbf{k}) + \int_{R_{\rm III}} \nabla_{\mathbf{k}} \times \mathbf{A}_{\rm III}(\mathbf{k})\right] \cdot \hat{\mathbf{z}} d^2\mathbf{k}$$
$$= \frac{1}{2\pi}\left[2\oint_{\Gamma_{\rm I}} \nabla_{\mathbf{k}}\psi(\mathbf{k}) \cdot d\mathbf{k}\right] = 2, \qquad (22)$$

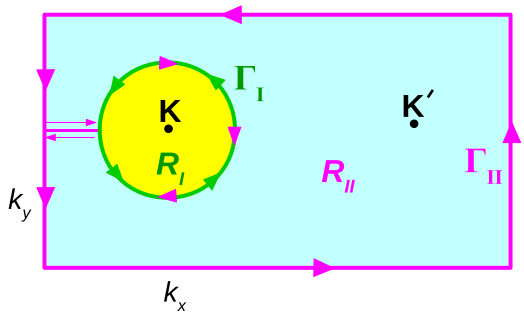

FIG. 6. Sketch of the FBZ with the locations of the singular points.

where we have taken the infinitesimal loop around $\mathbf{K}$ point to have the positive sense of rotation.

The Chern number for the valence band for all α as shown in Fig. 5 can be expressed as

$$\mathcal{C}_2(\alpha) = \Theta(1/\sqrt{2} - \alpha) + 2\Theta(\alpha - 1/\sqrt{2}) - \Theta(\alpha - \sqrt{2}).$$

The Chern number for the nondegenerate flat band turns out to be zero for all values of α i.e. $\mathcal{C}_1(\alpha) = 0$. Therefore the Chern number for the conduction band corresponding to $m = 0$ is $\mathcal{C}_0(\alpha) = -\mathcal{C}_2(\alpha)$. Using Eqs. (18) and (19), we have also calculated the Berry curvature and Chern numbers $\mathcal{C}_m$ numerically. Our numerical results support the exact analytical results. Figure 5 displays that the system undergoes a topological phase transition at $\alpha = 1/\sqrt{2}$ (also at $\alpha = \sqrt{2}$ due to the duality) since there is a change in the Chern number.

The anomalous Hall conductivity is directly related to the Chern number. When the Fermi energy is located in a band gap, the Hall conductivity can be expressed in terms of the Chern number as $\sigma_H = (e^2/h)\sum_m \mathcal{C}_m$, where m is restricted to the filled bands below the Fermi energy. By complete filling of the valence band or both the valence and flat bands, the system becomes a QHI with the Hall conductivity $\sigma_H = e^2/h$ for $\alpha < 1/\sqrt{2}$ and $\sigma_H = 2e^2/h$ for $1/\sqrt{2} < \alpha < \sqrt{2}$.

IV. CHIRAL EDGE STATES

In transport measurements through a mesoscopic two-dimensional system, the pair of edges parallel to the longitudinal current offers a sharp confining potential to the charge carriers in the transverse direction. As a result, the bulk 2D bands decompose into several 1D bands (or subbands) whose propagation vector is restricted along the longitudinal direction. The transport coefficients of a finite system is hence controlled by these subbands. The wave functions associated with these bands may be spread out in the bulk of the sample or localized at the edges.

The bulk-boundary correspondence (BBC) [14] tells that chiral edge states appear at the boundaries of a band insulator, if the Chern number of the 2D bulk band is nonzero. The number of the chiral modes along an edge is equal to the Chern number of the bulk band. These edge states show up in the 1D band structure as channels bridging the gap between the bulk bands. Since the irradiated α-$\mathcal{T}_3$ lattice is a Floquet-Chern insulator, it is expected to host topological edge states. We show the existence of chiral edge states by numerically computing the low-energy band structure of the α-$\mathcal{T}_3$ armchair nanoribbon driven by the off-resonant radiation (Fig. 7). The following parameters have been used: width of the ribbon $\approx$130 a, $\tau/\hbar\omega = 0.1$, and $J_1(\eta) = 0.8$. The edge states denoted by blue and red curves are localized at opposite edges of the ribbon. The slope of the edge bands determine the group velocity of the electronic states. Thus the edge states move with opposite group velocities at the two edges. They form a connection between the gapped bulk bands (black ensemble of curves). There is only one gapless edge band for $\alpha < 1/\sqrt{2}$ as shown in Figs. 7(a) and 7(b), consistent with the obtained Chern number shown in Fig. 5. On the other hand, Figs. 7(c) and 7(d) display that there are two edge bands for $\alpha = 0.8$ and $\alpha = 1$, which agrees with the calculated Chern

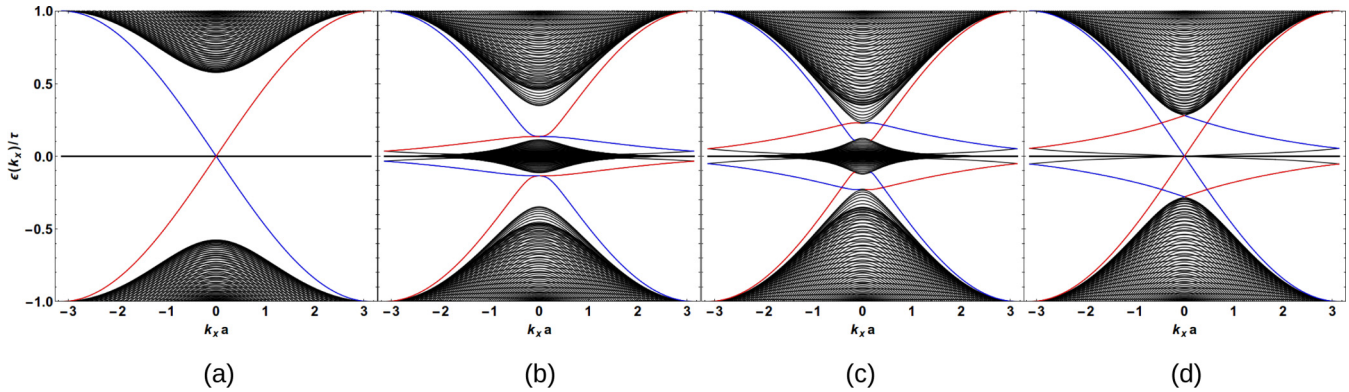

FIG. 7. Radiation-dressed band structure of the α-$\mathcal{T}_3$ nanoribbon with armchair edges for (a) $\alpha = 0$, (b) 0.5, (c) 0.8, and (d) 1.0. The red/blue curves represent edge states propagating on top/bottom edges, while the black curves represent the bulk bands.

number $\mathcal{C} = 2$. The BBC principle holds true in all these observations.

V. SUMMARY AND CONCLUSION

We have considered the α-$\mathcal{T}_3$ lattice illuminated by intense circularly polarized radiation of frequency much higher than the bandwidth of the system. Using the off-resonant approximation, we have derived exact analytical expressions of the effective static band structure over the full Brillouin zone. It is observed that the triple point degeneracy is completely lifted due to the broken TRS symmetry caused by circularly polarized light. It leads to unequal photoinduced gaps at **K** and **K**′ (except for monolayer graphene and dice lattice) due to the lack of inversion symmetry. At $\alpha = 1/\sqrt{2}$, the semimetalic phase is restored due to closing of gap between flat and valence bands at **K** and that between the conduction and flat bands at **K**′. The low-energy Dirac cones at **K** and **K**′ points resurface at the gap closing point. The gap-closing value of α is insensitive to the radiation amplitude and polarization of light (except linear) within the off-resonant approximation. The α-$\mathcal{T}_3$ lattice illuminated by the circularly polarized radiation is transformed to a Haldane-like Chern insulator. We find that there is a topological phase transition from the Chern number $\mathcal{C} = 1(0, -1)$ to a Chern number $\mathcal{C} = 2(0, -2)$ at the band closing point, where $\mathcal{C}$ is the Chern number of the valence (flat, conduction) band. This is an example of a three-band system having larger Chern number. The effect of nontrivial topology of the system should get reflected in the transport measurements through the chiral edge channels as shown for the armchair configuration.

ACKNOWLEDGMENT

We would like to thank Firoz Islam and Sonu Verma for useful discussion.

[1] K. von Klitzing, Rev. Mod. Phys. **58**, 519 (1986).
[2] M. Z. Hasan and C. L. Kane, Rev. Mod. Phys. **82**, 3045 (2010).
[3] X.-L. Qi and S.-C. Zhang, Rev. Mod. Phys. **83**, 1057 (2011).
[4] L. Lu, J. D. Joannopoulos, and M. Soljacic, Nat. Photon. **8**, 821 (2014).
[5] C. L. Kane and E. J. Mele, Phys. Rev. Lett. **95**, 226801 (2005).
[6] C. L. Kane and E. J. Mele, Phys. Rev. Lett. **95**, 146802 (2005).
[7] B. Bernevig, T. L. Hughes, and S. C. Zhang, Science **314**, 1757 (2006).
[8] F. D. M. Haldane, Phys. Rev. Lett. **61**, 2015 (1988).
[9] X. L. Qi, Y. S. Wu, and S. C. Zhang, Phys. Rev. B **74**, 085308 (2006).
[10] E. Tang, J. W. Mei, and X. G. Wen, Phys. Rev. Lett. **106**, 236802 (2011).
[11] K. Sun, Z. Gu, H. Katsura, and S. Das Sarma, Phys. Rev. Lett. **106**, 236803 (2011).
[12] T. Neupart, L. Santos, C. Chamon, and C. Mudry, K. Sun, Z. Gu, H. Katsura, and S. Das Sarma, Phys. Rev. Lett. **106**, 236804 (2011).
[13] G. Jotzu, M. Messer, R. Desbuquois, M. Lebrat, T. Uehlinger, D. Greif, and T. Esslinger, Nature (London) **515**, 237 (2014).
[14] Y. Hatsugai, Phys. Rev. Lett. **71**, 3697 (1993).
[15] A. P. Schnyder, S. Ryu, A. Furusaki, and A. W. W. Ludwig, Phys. Rev. B **78**, 195125 (2008).
[16] W. Yao, A. H. MacDonald, and Q. Niu, Phys. Rev. Lett. **99**, 047401 (2007).
[17] T. Oka and H. Aoki, Phys. Rev. B **79**, 081406(R) (2009).
[18] J. I. Inoue and A. Tanaka, Phys. Rev. Lett. **105**, 017401 (2010).
[19] T. Kitagawa, E. Berg, M. Rudner, and E. Demler, Phys. Rev. B **82**, 235114 (2010).
[20] T. Kitagawa, T. Oka, A. Brataas, L. Fu, and E. Demler, Phys. Rev. B **84**, 235108 (2011).
[21] N. Lindner, G. Refael, and V. Galitski, Nat. Phys. **7**, 490 (2011).
[22] B. Dora, J. Cayssol, F. Simon, and R. Moessner, Phys. Rev. Lett. **108**, 056602 (2012).
[23] G. Usaj, P. M. Perez-Piskunow, L. E. F. FoaTorres, and C. A. Balseiro, Phys. Rev. B **90**, 115423 (2014).
[24] J. W. Mclver, B. Schulte, F.-U. Stein, T. Matsuyama, G. Jotzu, G. Meier, and A. Cavalleri, arXiv:1811.03522.
[25] *Quantum Transport and Dissipation*, edited by T. Dittrich, P. Hanggi, G. L. Ingold, B. Kramer, G. Schon, and W. Zweger (Wiley-WCH, Weinheim, 1998).
[26] M. Vogl, P. Laurell, and A. D. Barr, arXiv:1808.01697.

[27] S. A. Skirlo, L. Lu, and M. Soljacic, Phys. Rev. Lett. **113**, 113904 (2014).
[28] S. A. Skirlo, L. Lu, Y. Igarashi, Q. Yan, J. Joannopoulos, and M. Soljacic, Phys. Rev. Lett. **115**, 253901 (2015).
[29] B. Sutherland, Phys. Rev. B **34**, 5208 (1986).
[30] J. Vidal, R. Mosseri, and B. Doucot, Phys. Rev. Lett. **81**, 5888 (1998).
[31] S. E. Korshunov, Phys. Rev. B **63**, 134503 (2001).
[32] M. Rizzi, V. Cataudella, and R. Fazio, Phys. Rev. B **73**, 144511 (2006).
[33] D. Bercioux, D. F. Urban, H. Grabert, and W. Hausler, Phys. Rev. A **80**, 063603 (2009).
[34] D. F. Urban, D. Bercioux, M. Wimmer, and W. Hausler, Phys. Rev. B **84**, 115136 (2011).
[35] J. D. Malcolm and E. J. Nicol, Phys. Rev. B **93**, 165433 (2016).
[36] M. Vigh, L. Oroszlany, S. Vajna, P. San-Jose, G. David, J. Cserti, and B. Dora, Phys. Rev. B **88**, 161413(R) (2013).
[37] F. Wang and Y. Ran, Phys. Rev. B **84**, 241103(R) (2011).
[38] A. Raoux, M. Morigi, J. N. Fuchs, F. Piechon, and G. Montambaux, Phys. Rev. Lett. **112**, 026402 (2014).
[39] J. D. Malcolm and E. J. Nicol, Phys. Rev. B **92**, 035118 (2015).
[40] E. Illes, J. P. Carbotte, and E. J. Nicol, Phys. Rev. B **92**, 245410 (2015).
[41] T. Biswas and T. K. Ghosh, J. Phys.: Condens. Matter **28**, 495302 (2016).
[42] A. D. Kovacs, G. David, B. Dora, and J. Cserti, Phys. Rev. B **95**, 035414 (2017).
[43] S. K. Firoz Islam and P. Dutta, Phys. Rev. B **96**, 045418 (2017).
[44] T. Biswas and T. K. Ghosh, J. Phys.: Condens. Matter **30**, 075301 (2018).
[45] B. Dey and T. K. Ghosh, Phys. Rev. B **98**, 075422 (2018).
[46] A. Iurov, G. Gumbs, and D. Huang, arXiv:1806.09172v2.
[47] D. O. Oriekhov, E. V. Gorbar, and P. Gusynin, J. Low Temp. Phys. **44**, 1313 (2018).
[48] D. O. Oriekhov, E. V. Gorbar, P. Gusynin, and D. O. Oriekhov, Phys. Rev. B **99**, 155124 (2019).
[49] Y.-R. Chen, Y. Xu, J. Wang, J.-F. Liu, and Z. Ma, Phys. Rev. B **99**, 045420 (2019).
[50] S. K. Firoz Islam, arXiv:1901.07943v1.
[51] M. Ezawa, Phys. Rev. Lett. **110**, 026603 (2013).
[52] K. Saha, Phys. Rev. B **94**, 081103(R) (2016).
[53] M. Tahir, A. Macchon, and U. Schwingenschlogl, Phys. Rev. B **90**, 125438 (2014).
[54] R. Liu, W.-C. Chen, Y.-F. Wang, and C.-D. Gong, J. Phys.: Condens. Matter **24**, 305602 (2012).
[55] M. Trescher and E. J. Bergholtz, Phys. Rev. B **86**, 241111(R) (2012).
[56] T. Andrijauskas, E. Anisimovas, M. Raciunas, A. Mekys, V. Kudriasov, I. B. Spielman, and G. Juzeliunas, Phys. Rev. A **92**, 033617 (2015).
[57] B. Jaworowski, A. Manolescu, and P. Potasz, Phys. Rev. B **92**, 245119 (2015).
[58] W. Magnus, Commun. Pure Appl. Math. **7**, 649 (1954).
[59] S. Blanes, F. Casas, J. A. Oteo, and J. Ros, Phys. Rep. **470**, 151 (2009).
[60] A. Lopez, A. Scholz, B. Santos, and J. Schliemann, Phys. Rev. B **91**, 125105 (2015).
[61] M. Kohmoto, Ann. Phys. (NY) **160**, 343 (1985).
[62] D. Xiao, M.-C. Chang, and Q. Niu, Rev. Mod. Phys. **82**, 1959 (2010).
[63] N. Goldman, G. Juzeliunas, P. Ohberg, and I. B. Spielman, Rep. Prog. Phys. **77**, 126401 (2014).
[64] T. Fukui, Y. Hatsugai, and H. Suzuki, J. Phys. Soc. Jpn. **74**, 1674 (2005).
[65] D. J. Thouless, M. Kohmoto, M. P. Nightingale, and M. den Nijs, Phys. Rev. Lett. **49**, 405 (1982).